

MEASUREMENT OF FLUENCE AND FLUX OF PROTON BEAMS USING DIFFERENTIALLY FILTERED DIAMOND DETECTORS AND RADIACHROMIC FILM

D. C. Judy, J. Blackburn, G. Merkel, R. M. Fleetwood
Army Research Laboratory, 2800 Powder Mill Rd., Adelphi, MD 20783-1197

D. M. Weidenheimer, B. Jenkins, S. G. Gorbics, N. R. Pereira
Berkeley Research Associates, PO Box 852, Springfield, VA 22150

Abstract

Differentially filtered, photoconductive, neutron-irradiated diamond detectors have been employed to investigate the temporal and energy distribution of an intense pulsed proton beam. Results were compared against measurements obtained using differentially filtered radiachromic film, electromagnetic (EM) techniques, time-of-flight techniques, and calorimetric instruments.

of conduction electrons, meaning that PCD's such as those described remain unsaturated even at high proton beam dose rates. The high capture rate of conduction electrons also explains the low sensitivity (bulk conductivity) and excellent time resolution of PCD detectors. [1-4]

I. INTRODUCTION

The measurement techniques discussed in this paper were designed to measure proton beam parameters which are of significance in thermostructural response investigations. Diamond detectors are particularly well suited for measuring the high dose rates that occur in soft x-ray and pulsed ion beam environments, up to 10^{14} rads(Si)/s. Further, they are rugged, exhibit excellent electrical and mechanical properties, and provide a sufficiently large signal to recommend their use in an energy spectrophotometer. The results of efforts to develop a four-channel diamond photoconductive proton energy spectrometer are discussed in this paper.

Four diamond photoconductive detectors (PCD's) with dimensions $(1.2)^2\text{mm}^2 \times 0.1$ mm were obtained from R. Wagner. [1] The detectors were fabricated by vacuum flashing gold electrodes onto the 0.1×1.2 mm² ends of the irradiated diamond and then cementing those ends to a mechanical support/terminal connection with conducting epoxy. Each was exposed to a neutron fluence of 2.15×10^{16} cm⁻² SDE (1 MeV silicon dose equivalent) The resulting interstitial damage determines the short lifetimes

The four channel PCD spectrometer was used in the characterization of the Aurora proton beam. The Aurora [5-8] accelerator at the Army Research Laboratory was the world's largest multi-megavolt proton generator usable for thermostructural response testing. The PCD spectrometer beam diagnostics were augmented by electromagnetic, stacked-filtered radiachromic film dosimetry and calorimetric techniques.

Aurora's proton beam exhibited a fluence nominally between 1 and 10 J/cm² over an area of about 1000 cm². Although stacked foil and other differential filtering techniques have been known for many years [9], further development to extend their suitability to the higher dose rate proton beams was required. For thermostructural response testing the relevant experimental value is dose as a function of depth. Dose rate as a function of depth is useful when proton fluence generates mechanical shock.

II. DIAMOND PHOTOCONDUCTIVE DETECTORS

The radiation response of diamond photoconductive detectors can be understood in terms of a simple model. In general, there are two distinct extreme cases when considering PC

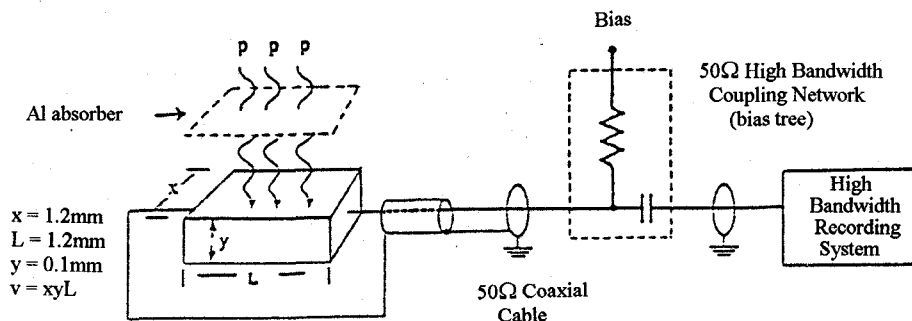


Figure 1. Electrical setup of diamond detectors. Because the detector acts as a resistor, current through the device produces a voltage drop that reduces the potential current drawn by the detector. Therefore, the measured response, V_m , is corrected by $V_c = V_m / (1 - V_m / \text{Bias})$. If Bias is large, the correction is insignificant. [4]

Detector responsivity: volume absorbed radiation, and surface absorbed radiation. In the case of homogeneous depth absorption (e.g. high energy gamma rays) [1]

$$I/\dot{D} = q \mu^* \rho \tau (\text{Vol})V/(L^2W), \quad (1)$$

where I is the detector current, \dot{D} is the radiation flux in rads(C)/sec, q is the electronic charge, μ^* is the electron drift velocity, τ is the carrier relaxation time, ρ is the density of the semi-conductor, (Vol) is the semi-conductor active volume, L is the contact spacing on the detector, W is the average energy to create an electron-hole pair in the semiconductor (approx. 5.5 eV for diamond), and V is the voltage across the PCD. When the incident radiation has a range less than the detector thickness, it can be shown that [1]

$$I/P = q \mu^* \rho \tau V/(L^2W) \quad (2)$$

where P is the incident beam power. If the diamond is thick enough to stop the proton beam, the latter equation applies. If

not, the inhomogeneous absorption as a function of depth must be taken into consideration.

III. PROTON BEAM TEST BED

Figure 2 shows the experimental arrangement designed to produce the proton beam. The closely spaced filtered PCD diamonds (maximum distance between PCDs 2 cm) could be located at various positions in the drift tube. One of these positions is indicated in figure 2. EM measurements are made at the various places indicated. Ion current is measured using three azimuthal distributed B-dot sensors labeled BDCIn ($n = 1-3$), and positioned at the diode exit. Voltage is determined from self-integrating electric field sensors marked EKCC. Electrons are emitted from a cylindrical cathode and impinge on a 2-mil polyethylene foil, ionizing the foil and producing protons. Slow-moving protons are accelerated longitudinally in the opposite direction from the electron flow. The relationship between the electrons and protons is described in Figure 3. [10]

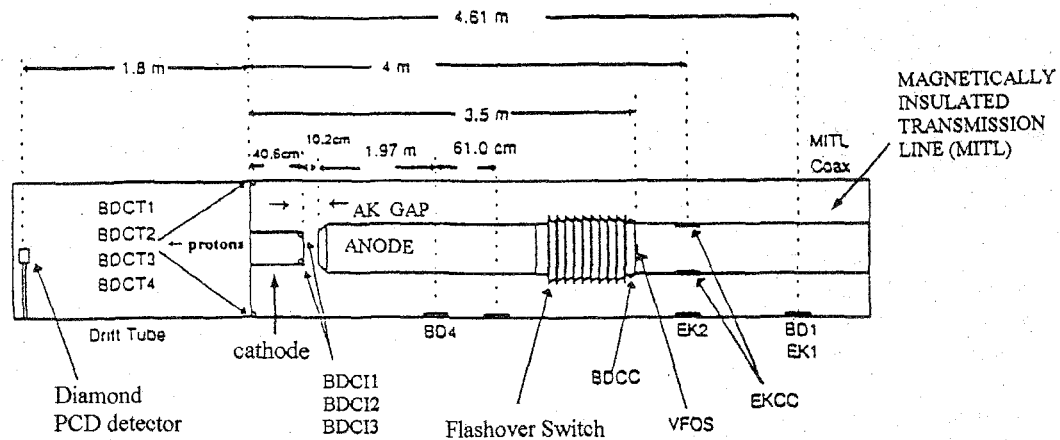


Figure 2. Experimental setup (not to scale)(Direction of Protons ←). Arrows point to the sensors. The B-dot sensors are designated by the two letters BD. The sensors BDCI1, BDCI2, and BDCI3 measure ion current at the cathode. Other BD sensors measure total current. The sensors marked with the first letter E are E-dot sensors. The sensor marked "VFOS" measures the flashover switch voltage drop. The diamond PCDs are marked "Diamond PCD detector".

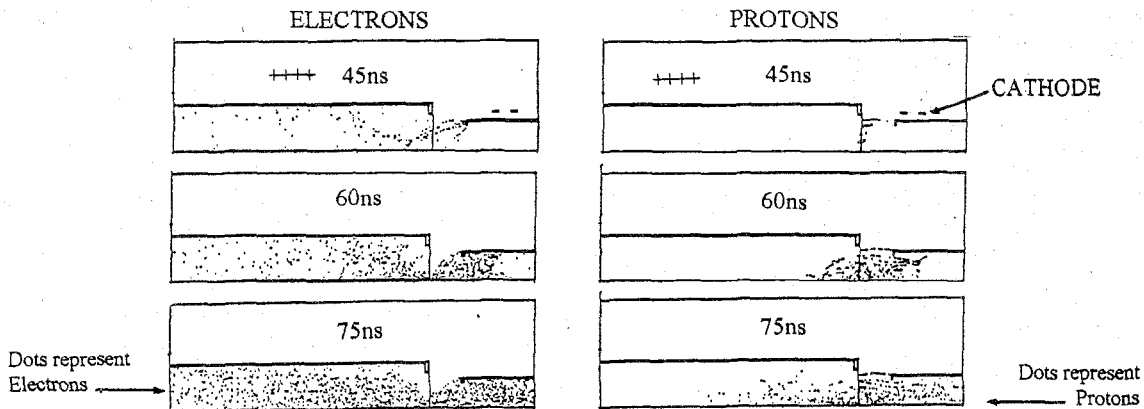


Figure 3. MAGIC particle-in-cell calculations of electron and proton swarms during a typical Aurora shot for diode shown in Figure 1. The electrons are emitted from the cathode and ionize the hydrocarbon foil to produce protons which slowly accelerate in the opposite direction.

IV. PCD MEASUREMENTS

Figures 4a and 4b show typical electrical signals. The traces in figure 4a are the diode voltage (dotted line) right scale and the ion current (solid line) left side. The ion current was obtained by averaging over the 3 B-dot EM probes BDCI(1-3), positions shown in figure 2. The signals in 4b are the total ion dose rate from an unfiltered diamond PCD (solid line, left scale): the dotted line is the product of the diode voltage with the ion current (from BDCIns), or the power in the ions (right scale). The ion power is qualitatively similar to the ion dose rate, but shifted in time by 100 ns, corresponding to a typical ion velocity of $31 \text{ m}/\mu\text{s}$ or $\beta = 0.1$, and an ion energy 5.0 MeV . The dose rate increases faster than the ion power because of time-of-flight pulse compression.

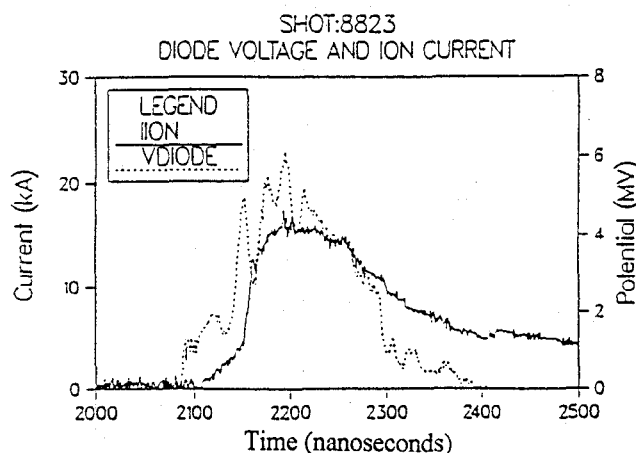


Figure 4a. Diode voltage and ion current for shot 8823. The traces are the diode voltage (dotted line, right scale) and the ion current (left scale), obtained by averaging the 3 B-dot EM probes, BDCI(1-3), positions shown in Figure 2.

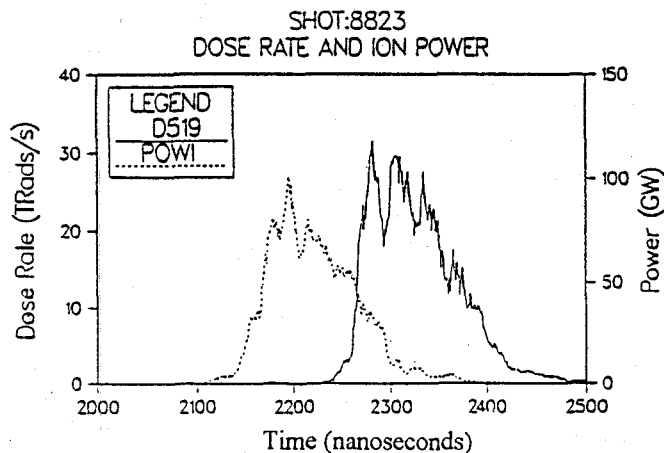


Figure 4b. Ion dose rate measured with thick PCD detector and diode power calculated from current and voltage in figure 4a.

Figure 5 shows signals produced by three PCDs arranged in close spatial proximity, and shielded behind a $7 \text{ mg}/\text{cm}^2$ absorber. The differences in the pulses can be attributed to a combination of sensor sensitivity variation combined with spatial variations.

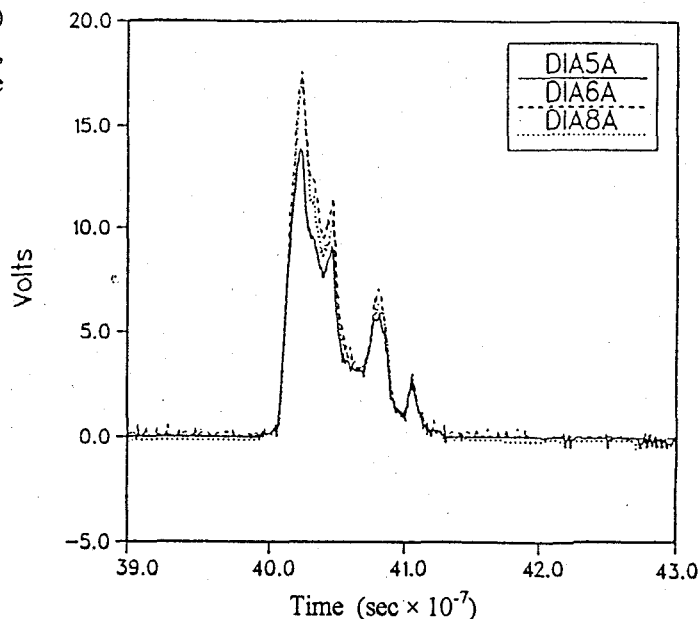


Figure 5. Response of three PCD thin-diamond detectors exposed to the same beam, each with a $7 \text{ mg}/\text{cm}^2$ Al absorber. Variations in pulse height can be due to differences in detectors or to beam spatial inhomogeneities.

Figure 6a illustrates a similar measurement obtained during a different shot using four diamond detectors shielded behind four absorbers of varying thicknesses, specifically, 0.0 , 21.5 , 34.7 and $50.6 \text{ mg}/\text{cm}^2$ Al. Pulse width for lightly filtered PCDs is much larger than for more heavily filtered ones. Also, peak signal decreases with increasing filter thickness. Clearly, energetic ions capable of penetrating the thickest filter are present for only short durations, while less energetic ions penetrating into detectors shielded by lighter filters comprise more of the pulse. For example, the pulse width seen behind a $21.5 \text{ mg}/\text{cm}^2$ filter is about 50 ns . A pulse width of 3 ns is measured behind the $50.6 \text{ mg}/\text{cm}^2$ filter.

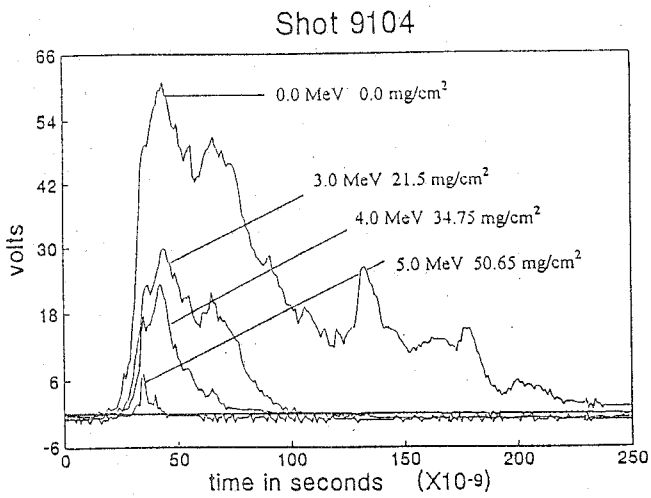


Figure 6a. Four diamond PCDs with different filters exposed to the same beam.

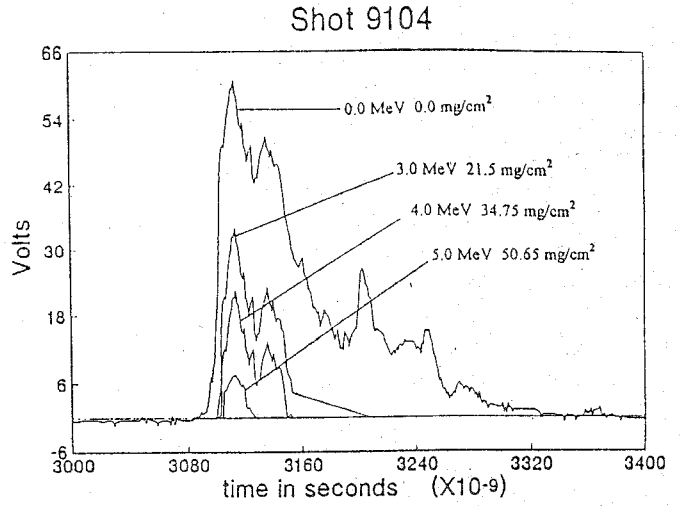
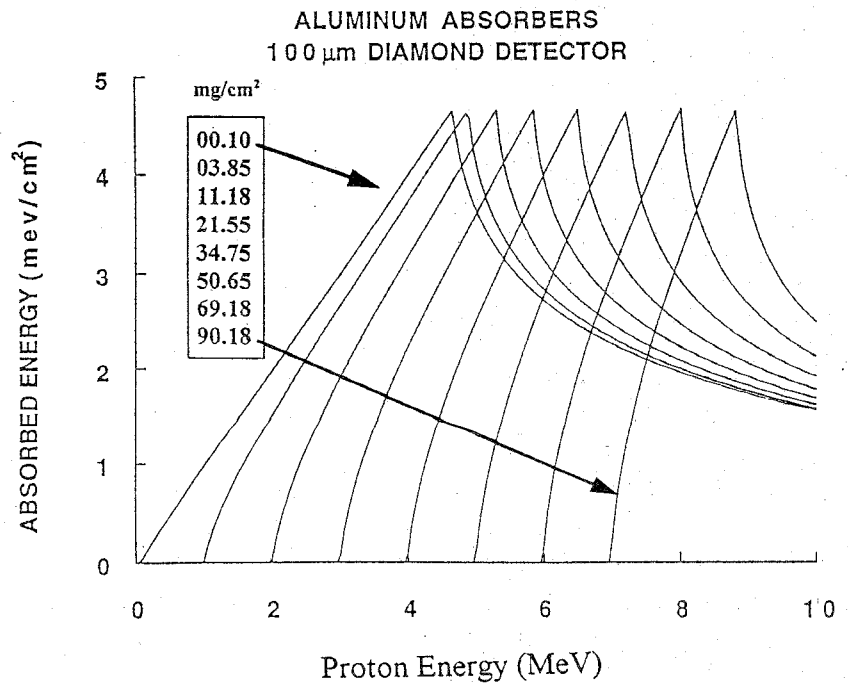


Figure 6b. Calculated response of diamond PCDs.

Figure 6b shows the calculated response of the four PCDs if we assume that the measured voltage across the diode determines the kinetic energy of the protons in the proton beam. More than four diamond detectors would be required to unfold a precise temporal energy spectrum such as discussed in Section VI.

Figure 7 shows the response functions for these and other filter-detector combinations. The 21.5 mg/cm² Al filter gives a response threshold at 3 MeV, 34.75 mg/cm² gives 4 MeV, and 50.6 mg/cm² gives 5 MeV. Therefore, the energy exceeds 3 MeV for at least 50 ns.

Figure 7. Response curves of filtered diamond detectors to protons. Sharp peaks occur when the energy of the proton is such that the trajectory of the proton does not end in the PCD. If the proton has enough energy so that the trajectory of the proton passes right through the PCD, the large deposition of ionizing energy into the PCD due to the Bragg peak does not occur.



V. RADIACHROMIC STACKED FOIL MEASUREMENTS

Up to this point we have limited our discussion to temporal proton distributions. We can cross check our results and obtain information on integrated pulse energy or dose by employing stacked radiachromic films and calorimetry measurements.

Radiachromic-proton dosimetry measurements [11,12] on the depth-dose profile of the proton beam were made using a stack of aluminum foils sandwiched between radiachromic nylon films. The dose in the film is determined from the change in optical density, OD, measured at two wavelengths, i.e. 6000 and 5100Å.

Far West Technology, Inc., (FWT) of Goleta, CA [12] provided very thin (approximately 1 mg/cm^2 or $10 \text{ }\mu\text{m}$) radiachromic films that allowed up to 20 foils/films in a sandwich stack (Figure 8).

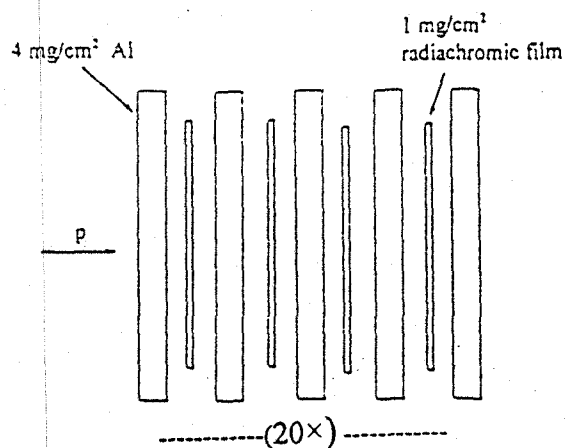


Figure 8. Stacked foil dosimetry sandwich. The first foil could be Al or a radiachromic film. Up to 20 iterations were utilized.

One of the main objectives of this study was to ascertain if the same dose (energy/mass) deposited by a ^{60}Co gamma source or other low dose-rate source (as usually used for film calibration) produced the same radiachromic film response as the high dose-rate Aurora ion source. [11,12]. Obviously there are limits to the span in dose rate magnitude than can be measured with the

radiachromic films. Our ^{60}Co source irradiation took a long time (36 hrs of exposure to produce 10 Mrads), whereas the high-current Aurora ion-beam pulse could deliver the same dose in 100 ns.

Another independent dose calibration was obtained with the proton beam produced by the Naval Surface Weapons Center (NSWC) Pelletron. Figure 9 shows calibration points obtained with ^{60}Co gamma rays and protons produced by the (NSWC) Pelletron. The Pelletron data corresponds to 2- and 4-MeV protons. Bombardment with He ions on another radiachromic film batch resulted in similar results. Agreement between the ^{60}Co and Pelletron data is within 20 percent. The calibration supplied by the manufacturer, (FWT), corresponding to a different film batch, is substantially different. However, FWT advises users of the film that each film batch should be independently calibrated. (See sections VII and VIII for comparisons with high dose rate AURORA beam measurements.)

VI. INTERPRETATION OF STACKED FOIL DOSIMETRY MEASUREMENTS

Three Aurora proton-beam depth-dose profile measurements obtained with stacked foils are shown in figure 10. The 2" anode-cathode (AK) gap results in a lower diode impedance than the 5" AK gap. A high impedance diode has a higher voltage across it and therefore accelerates the protons to a higher energy. High energy protons produce a deeper dose-depth profile.

RADIACHROMIC FILM CALIBRATION CURVE

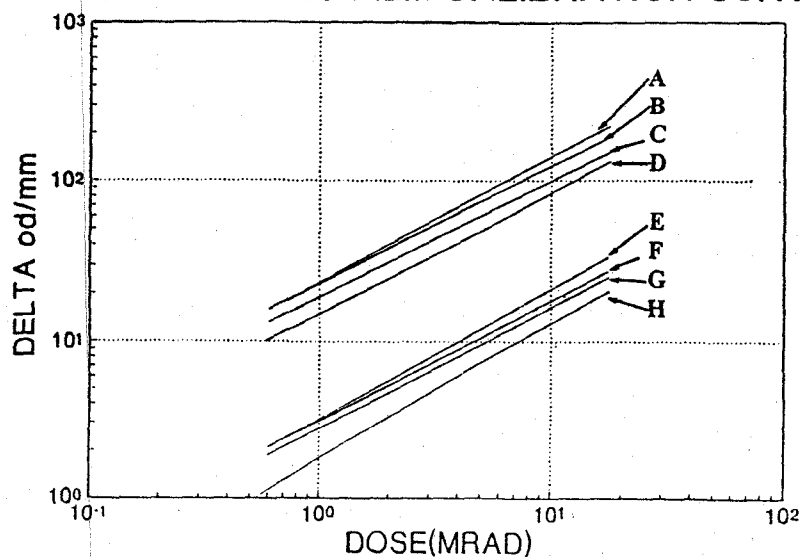


Figure 9. Radiachromic film calibration curves: Curves marked A, B, C, D correspond to 600 nm wavelength absorption; the Curves E, F, G, H to 510 nm wavelength absorption. Curves A and E correspond to calibrations with 4 MeV protons - Curves B and F with 2 MeV protons - Curves C and G with a cobalt source and finally, Curves D and H are nominal calibrations supplied by FWT with the statement that "every batch of film should be recalibrated because there is a batch to batch shift on the log-log plots".

Delta od/mm corresponds to the change in optical density divided by foil thickness in mm.

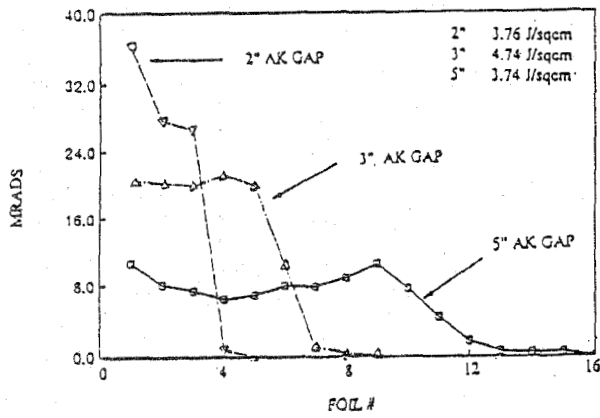


Figure 10. Stacked foil depth-dose plots obtained for 3 different AK settings. (See Fig. 2).

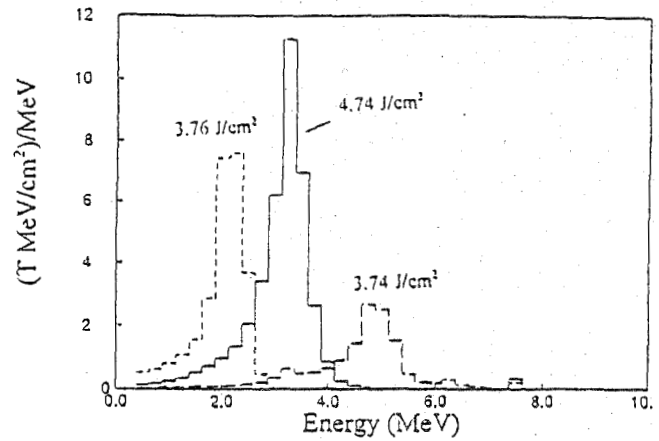


Figure 12. Three examples of unfolded stacked foil depth-dose data (figure 10) corresponding to the 2", 3", and 5" AK Gaps shown in figure 10.

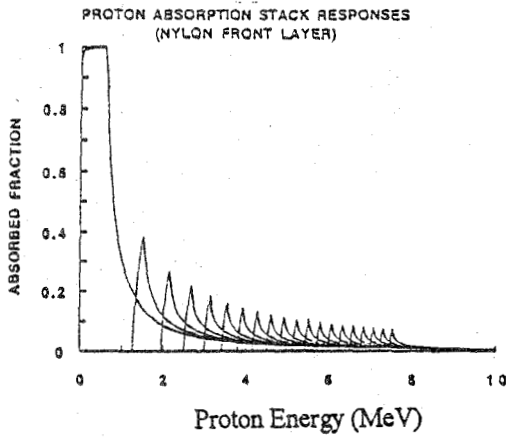


Figure 11. Relative response of radiachromic films in 20 foil absorption sandwich.

The stacked-foil measurements can be interpreted by "unfolding" [13] to yield the energy distribution of the proton-beam density as a function of proton-beam energy. Figure 11 shows the calculated relative response of stacked-foil, aluminum-radiachromic-foil sandwiches for various proton energies, and figure 12 shows three Aurora proton-beam energy distributions derived from measurements of the type shown in figure 10, interpreted via figure 11. The different energy distributions in figure 12 correspond to the anode-cathode gaps in figure 10. The distribution of the kinetic proton energy determined by stacked foils can be compared to proton kinetic energy corresponding to the diode voltage, figure 13.

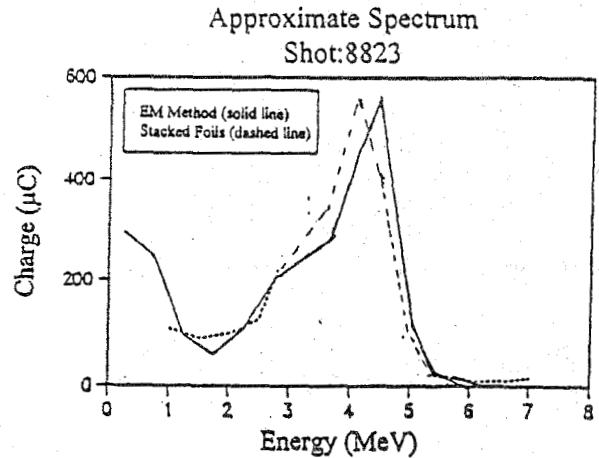


Figure 13. Comparison between proton energy distribution derived from electromagnetic measurements and those derived from stacked foil measurements.

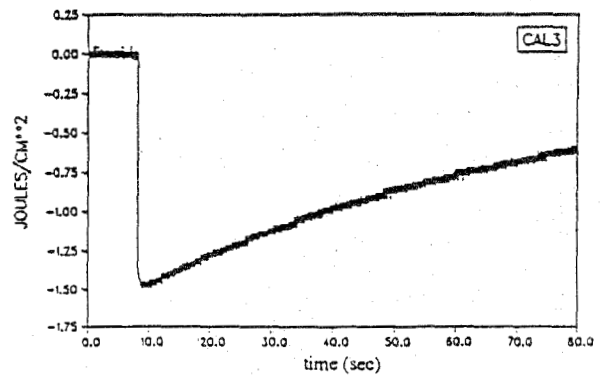


Figure 14. Calorimeter measurement curve. The decay corresponds to cooling of calorimetric foil.

VII. CALORIMETRY MEASUREMENTS

Figure 14 shows a digitizer trace corresponding to a typical calorimeter measurement. The decay of the curve in this figure corresponds to the temperature loss of the tantalum calorimeter foil as a function of time. Table I compares a number of stacked-foil energy measurements with calorimetry measurements obtained adjacent to the stacked foil.

TABLE I

Shot#	AK Gap	Calorimeter 1 J/cm ²	Film on calorimeter 1 J/cm ²	Ratio of film to calorimeter measurement
9019	4"	1.280	1.790	1.398
9020	4"	1.740	2.400	1.379
9021	4"	0.840	0.808	0.962
9022	4"	2.130	3.590	1.685
9023	4"	1.600	1.760	1.100
9024	4"	0.888	1.040	1.172
9025	4"	0.815	0.717	0.879
9026	3"	0.524	0.659	1.258
9027	3"	0.840	0.742	0.883
9028	3"	1.260	1.240	0.984
average ratio 1.170		standard deviation 0.260		

VIII. COMPARISON OF RADIACHROMIC AND EM MEASUREMENT

The total incident fluence or energy was determined by measuring a spatial distribution of dose (measured by radiachromic film) along the radius of the drift tube about 2 meters from the diode. The dimensions of the vertical radial distribution and the partial horizontal distribution of the radiachromic film positions are shown in figure 15. Figure 16 shows plots of horizontal and vertical distributions of dose measurements. The dotted line corresponds to vertical distribution measurements, the dashed line corresponds to folded horizontal measurements. The solid line is a curve fit to the measurements. By integration, the total dose corresponds to :

$$2\pi \left(\int_0^{50\text{cm}} e(r) r dr \right) = 7.4 \times 10^3 \text{ joules.} \quad (3)$$

The corresponding electromagnetic measurements for the same Aurora shot yielded 6.9×10^3 joules.

EM measurements of the proton beam current and diode voltage can be analyzed to yield the power of the incident proton beam. Figure 17 shows the measured proton current and diode voltage. The diode voltage was determined by subtracting the

voltage across the flash-over switch from the voltage measured just upstream by the sensor marked EKCC. The product of the voltage and ion current or incident beam power is shown in figure 18. The total beam power can then be related to the total integrated dose. For the particular AURORA shot analyzed, ion incident energy determined from the integrated power pulse was 6.9×10^3 joules. As already indicated, the agreement was within 5% of the results i.e. calculated from data shown in figure 16.

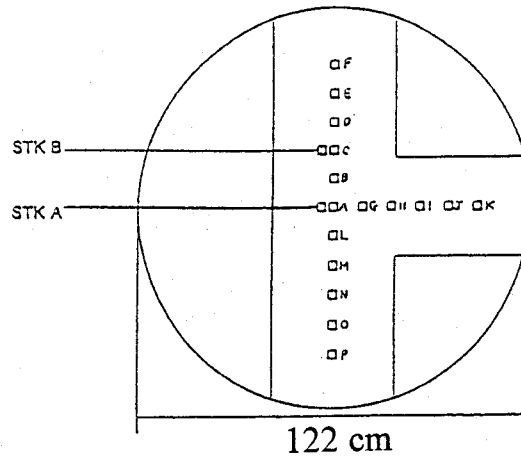
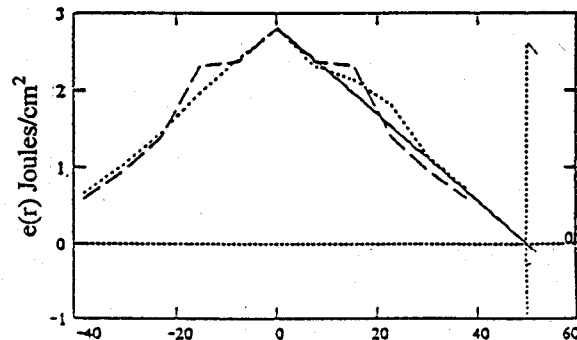


Figure 15. Radiachromic foil spatial distribution employed to obtain total integrated dose of proton beam. The vertical distribution is across the entire diameter. The horizontal distribution is across one half of the diameter.



Vertical and horizontal positions in cm.

Figure 16. Triangular fit to total dose measurement obtained with geometry shown in figure 15. The dashed line corresponds to horizontal measurements, the dotted line to vertical measurements. (The horizontal distribution is insignificant beyond ± 50 cm).

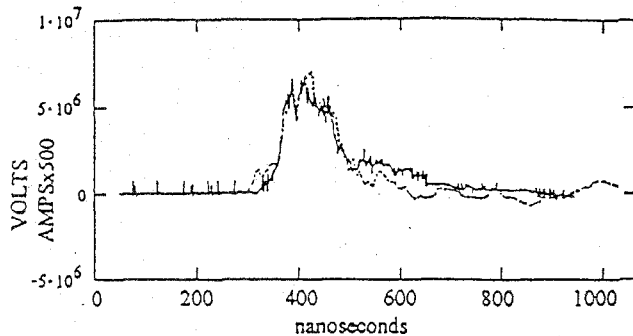


Figure 17. Diode voltage and proton current in volts and amps. The solid line corresponds to the current and the dotted line to the voltage.

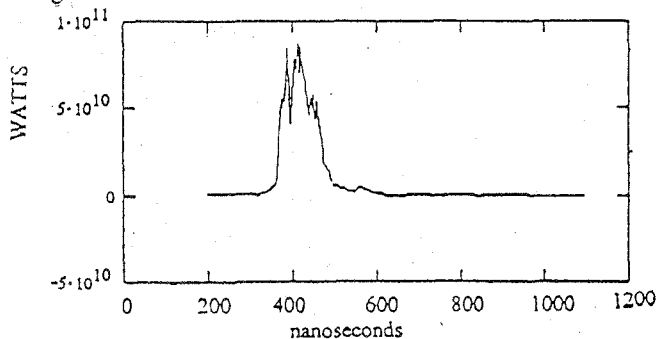


Figure 18. Diode proton beam power in joules.

IX. CONCLUSIONS

Neutron irradiated [subjected to a neutron flux of $2.15 \times 10^{16} \text{ n/cm}^2 \text{ 1 MeV SDE}$] diamond photoconductive detectors (PCDs) can be employed to investigate the energy distribution of proton beams corresponding to dose rates of $10^{14} \text{ rads(Si)/sec}$. Filtered diamond PCDs can also be used to yield the temporal kinetic energy distribution of the protons in the beam. The dose-depth profiles produced by the ion beam were controlled by changing the Aurora AK proton beam gap. The electromagnetic determination of the proton ion beam power, when integrated, agreed with the total proton beam energy determined by radiachromic film measurement within 5%. Radiachromic dose-depth measurements were within $\pm 20\%$ of the electromagnetic and calorimetric measurements giving added confidence in the measurements. (The radiachromic films were calibrated with ^{60}Co sources, over a period of 36 hours. The proton beam dose was delivered in about 150 ns.) In general, stacked-foil measurements can be used to obtain dose-depth distributions as a function of position and AK gap. The filtered diamond PC detectors yield temporal and spatial distributions of depth dose rate.

The parameters of the proton beam produced by the Aurora accelerator (such as total energy, power, current, proton kinetic energy) could be controlled by changing the pulse width (crow-baring), changing the diode AK gap and changing the Marx charging voltage. The measurement techniques described here

can successfully be combined to achieve the characterization of proton beam parameters of significance in thermostructural response investigations.

References:

1. R. S. Wagner, J. H. Bradley, and R. B. Hammond, "Picosecond Photoconductors as Radiation Detectors," *IEEE Trans. Nucl. Sci.*, NS-33, No. 1, p. 250, February 1986.
2. R. S. Wagner, J. R. Joseph, R. A. Hilko, R. W. Harper, J. R. Tinsley, "The Temporal Response and Relative Proton-To-Gamma Ratio of Radiation Detectors Made From Natural Diamond," *Conference on Application of Accelerators in Research and Industry*, Denton, TX, 1992.
3. Rick B. Spielman, "A Five-channel, Diamond Photoconducting X-ray Detector Array for Z-pinch Experiments," *Rev. Sci. Instrum.* **63**(10), p. 5066, October, 1992.
4. R. B. Spielman, W. W. Hsing, and D. L. Hanson, "Photoconducting x-ray detectors for Z-pinch Experiments," *Rev. Sci. Instrum.*, **59**(8), p. 1804, August 1988.
5. Bernstein, B. and I. D. Smith, "Aurora, An Electron Accelerator," *IEEE Trans. Nucl. Sci.*, NS-20, p. 294, June, 1973.
6. G. Merkel, M. Litz, H. Roberts, M. Smith, G. W. Still, R. B. Miller, W. F. McCullough, "Behavior of a Relativistic electron Beam in a Gas-Filled Drift Tube as a Function of Gas Pressure," *IEEE Trans. Nucl. Sci.*, NS-40, p. 1434, December 1993.
7. R. B. Miller, W. F. McCullough, G. Merkel, M. Litz, H. Roberts, M. Smith and G. W. Still, "Risetime Sharpening Using Magnetic Insulation in the Aurora Diode," *IEEE Trans. Nucl. Sci.*, NS-40, p. 1426, December 1993.
8. M. Bushell, R. Fleetwood, D. Judy, G. Merkel, M. Smith, K. Nguyen, D. Weidenheimer, "Bremsstrahlung Risetime Shortening by Diode Geometry Reconfiguration," *IEEE Trans. Nucl. Sci.*, NS-39, p. 2070, December 1992.
9. E. L. Kelly and E. Segrè, "Some Excitation Functions of Bismuth," *Phys. Rev.* **75**(7), p. 999, April, 1949.
10. B. Goplin, L. Ludeking, J. McDonald, G. Warren, and R. Worl, "Magic User's Manual," *Mission Research Corp, Report MRC/WDC-R-184*, 1988.
11. W. L. McLaughlin, "Radiachromic dye-cyanide dosimeters," in *Manual on Radiation*, N. W. Holm and R. J. Berry, Eds., New York, Marcel Decker, 1989, p. 377.
12. The thin radiachromic films were supplied by Far West Technology, Inc., "FWT Radiachromic Radiation Measurement, Material and Readers Manual," Far West Technology, Inc. 330-D South Kellogg, Goleta, CA 93117.
13. S. G. Gorbics and N. R. Pereira, Differential Absorption Spectrometer for Pulsed Bremsstrahlung, *Rev. Sci. Instrum.* **64**, p. 1835, 1993; For a general discussion of unfolding, see I. J. D. Craig and J. C. Brown, *Inverse Problems in Astronomy*, (Hilge, Bristol, 1986); widely used unfolding codes based on matrix methods include STAY'SL (F. Perry, ORNL/TM-6062, 1977), and LSL (F. W. Stallman, NUREG/CR-0029, 1983). These codes are available from the Radiation Shielding Information Center, ORNL.